How tobacco (Nicotiana tabacum) BY-2 cells cope with Eu(III) – A microspectroscopic study.

Klotzsche, M.; Vogel, M.; Sachs, S.; Raff, J.; Stumpf, T.; Drobot, B.; Steudtner, R.;

Originally published:

August 2023

Analyst 148(2023)19, 4668-4676

DOI: https://doi.org/10.1039/D3AN00741C

ARTICLE

How tobacco (*Nicotiana tabacum*) BY-2 cells cope with Eu(III) – A microspectroscopic study

Received 00th January 20xx,
Accepted 00th January 20xx

DOI: 10.1039/x0xx00000x

Max Klotzsche,[a] Manja Vogel,[b] Susanne Sachs,[a] Johannes Raff,[a] Thorsten Stumpf,[a] Björn Drobot,[a] Robin Steudtner,[a*]

The extensive use of lanthanides in science, industry and high-technology products is accompanied by an anthropogenic input of rare earths into the environment. Knowledge of the metal's environmental fate is essential for a reasonable risk assessment and remediation approaches. In the present study, Eu(III) was representatively used as luminescent probe to study the chemical environment and to elucidate the molecular interactions of lanthanides with a suspension cell culture of *Nicotiana tabacum* BY-2. Biochemical methods were combined with luminescence spectroscopy, two-dimensional microspectroscopic mappings, and data deconvolution methods to resolve bioassociation behavior and spatial distribution of Eu(III) in plant cells. BY-2 cells were found to gradually take up the metal after exposure to 100 µM Eu(III) without significant loss of viability. Time-resolved luminescence measurements were used to specify the occurrence of Eu(III) species as a function of time, revealing the transformation of an initial Eu(III) species into another after 24 h exposure. Chemical microscopy and subsequent iterative factor analysis unveil the presence of four distinct Eu(III) species located at different cellular compartments, *e.g.* the cell nucleus, nucleolus and the cell walls, which could be assigned to intracellular binding motifs. In addition, a special type of bioaccumulation occurs through the formation of a Eu(III)-containing oxalate biomineral, which is already formed within the first 24 hours after metal exposure. Oxalate crystals were also obtained in analogous experiments with Gd and Sm. These results indicate that tobacco BY-2 cells induce the precipitation of metal oxalate biominerals for detoxification of lanthanides, although they also bind to other cellular ligands at the same time.

1. Introduction

Lanthanides (Ln) have become essential for modern life due to their unique chemical, optical, luminescent and magnetic properties. Based on their electronic structure, they can be utilized in a variety of scientific and industrial purposes. Nowadays Ln are found as active sites in catalysts for oil refining and exhaust gas treatment, as phosphors for lighting and lasers, in magnets for electric cars and wind turbines, in biomedical imaging and agriculture.[1,2] At the same time, the widespread use of Ln is leading to increased inputs of these elements into the environment due to mining activities followed by water and air flows from tailing dumps and sites of further processing as well as the use of Ln-containing fertilizers.[3–5] A high mobility might cause an increase of Ln concentrations in aquatic and terrestrial ecosystems in the vicinity of entry sites. In fact, diverse exposure scenarios occurring in the environment have led to positive anthropogenic Ln anomalies in geo-, hydro- and biosphere, *e.g.* increased Gd levels in river systems from medical wastewater.[6–8] These micropollutions become available to living organisms by migration through the soil and groundwater, thus raising concerns about their toxicity and impacts on ecosystems worldwide. Although being non-essential elements for plants, Ln are absorbed by plant roots and transported to green plant parts. Ingestion of Ln-containing edible plant parts poses only one possible route of entry into the food chain of animals and humans and might potentially compromise human health.[9,10] A lack of data on Ln toxicity to living organisms underlines the necessity to comprehensively understand the molecular processes associated with uptake and accumulation of these elements into plants. Additionally, trivalent Ln serve as non-radioactive chemical analogues for trivalent radioactive actinides (An), based on comparable ionic radii and a similar aqueous chemistry. The knowledge of uptake and accumulation mechanisms is not only crucial for the risk assessment of biospheres exposed to exogenous Ln and An entry and to determine the threats to food safety and human health. Also, bioremediation of radioactively and/or metal contaminated areas by plants constitutes a cost-effective and environment-friendly approach to reclaim soil from the dismantling of nuclear facilities in order to decrease the amount of waste to be disposed in a deep geological repository.

Ln uptake strongly depends on their bioavailability, which in turn is influenced by speciation, *i.e.* the physico-chemical form, of the metal.[11] In the course of ordinary homeostasis, the uptake pathway for essential metal ions, *e.g.* Fe, Cu and Zn, might also be open for Ln ions, thus entering the organism and

[a] *Helmholtz-Zentrum Dresden-Rossendorf e.V., Insitute of Resource Ecology, Bautzner Landstraße 400, 01328 Dresden, Germany*
[b] *VKTA – Strahlenschutz, Analytik & Entsorgung Rossendorf e.V., Bautzner Landstraße 400, 01328 Dresden, Germany*
† Footnotes relating to the title and/or authors should appear here.
Electronic Supplementary Information (ESI) available: [details of any supplementary information available should be included here]. See DOI: 10.1039/x0xx00000x

triggering a broad range of physiological and metabolic alterations.[12] One major reason for the impairment of ordinary plant metabolism is the competition between non-essential trivalent Ln ions and essential metal ions because of their similar ionic radii, as in the case of Ca(II), Na(I) and Cu(I), or charge, as in the case of Fe(III). Non-essential elements can modify the active conformation of biomolecules, alter the structural integrity of proteins and decrease enzyme activity by displacing essential metal ions from their respective protein binding sites, leading to a modification or even interruption of the protein's functioning.[13–15] Nevertheless, rare earth element (REE) addition to growing plants does not necessarily lead to adverse health effects. In fact, the application of Ln(III)-bearing fertilizers is a common agricultural technique in China, increasing crop yields and quality for certain plants.[16] Low concentrations of La are reported to stimulate photosynthetic rate and plant biomass in soybean and 25-100 µM Ce are reported to stimulate germination and growth of rice plants. Higher concentrations of these elements, in turn, lead to reduced biomass growth and inhibitory affects.[17,18]

Generally speaking, plants possess a wide range of homeostatic mechanisms to cope with metal stress, mainly based on sequestration and efflux.[19] Different plant species have developed various mechanisms to transport potentially toxic metals to subcellular compartments for harmless storage. Vacuolar compartmentalization is a well-documented example to reduce the concentration of heavy metals in the cytosol and has been investigated thoroughly for Cd, Zn, Cu, Fe and Mo.[20–23] The uptake, chelation, sequestration, mineralisation and secretion of Ln in plant cells on the other hand is still a conflicting subject in current literature. In the past it was assumed that Ln are only deposited in the apoplast and do not enter plant cells,[24–26] whereas more recent studies indicate bioaccumulation in chloroplasts, vacuole, membranes, cell walls and nucleus.[27–30] However, the underlying uptake mechanisms and molecular interactions of Ln with biological molecules in plants still need to be uncovered. In this regard, plant cells in a suspension culture are a suitable approach to study physiological and biochemical mechanisms with control over nutrient supply and growth conditions. Cell cultures of *Brassica napus*, *Daucus carota* and *Nicotiana tabacum* have already been utilized to study the cytotoxicity and bioassociation of Cm(III), U(VI) and Eu(III) under biochemical, metabolic and spectroscopic aspects.[29,31–35] Among a multitude of cell lines derived from higher plants, suspension cell cultures of *Nicotiana tabacum* L. cv. Bright Yellow-2 (BY-2) are widely used because of their high growth rate, high homogeneity and modest cultivation in the laboratory.[36] While BY-2 cells have been used to study the phytotoxicity of pharmaceuticals, the stress response in the presence of heavy metals, their interaction with actinides, or the effects of various types of nanoparticles on cell ,[33,34,37–42] reports on the effect of Ln on cell metabolism and integrity as well as metal uptake and distribution remain scarce.

In the present study we used tobacco (*Nicotiana tabacum*) BY-2 suspension cells to investigate the interaction of Eu(III) as a luminescent probe (further details in electronic supplementary information (ESI, **Fig. S 1**) and representative for trivalent Ln with plants on a molecular level. The uptake of Eu(III) was tracked by inductively coupled plasma mass spectrometry (ICP-MS) and phytotoxicity was examined by viability assays. Time-resolved laser-induced fluorescence spectroscopy (TRLFS) gave access to metal speciation changes on a macroscopic level. This was supplemented by chemical microscopy, which further resolved the spatial distribution of Eu(III) in the cells on a microscopic level.

2. Materials and methods

2.1. Cultivation of tobacco BY-2 cell culture

Tobacco (*Nicotiana tabacum*) Bright Yellow-2 (BY-2) cells were provided by the Botanical Institute of the Karlsruhe Institute of Technology and cultivated as outlined by Rajabi *et al.*[34] in a modified liquid Murashige and Skoog (MS) medium, containing 4.3 g L^{-1} MS basal salt, 200 mg L^{-1} KH_2PO_4, 30 g L^{-1} sucrose, 100 mg L^{-1} myo-inositol, 1 mg L^{-1} thiamine hydrochloride and 0.2 mg L^{-1} 2,4-dichlorophenoxyacetic acid. After preparation the pH of the medium was adjusted to 5.8 with 1 M KOH and the medium was autoclaved for 20 min at 121 °C. The cells were grown at 25 °C in the dark on an orbital shaker at 150 rpm. Continuously, subcultivation was performed after seven days by transferring 1 mL of cell suspension into a sterile 100 mL Erlenmeyer flask filled with 30 mL fresh MS medium.

2.2. Eu(III) exposure and viability assay of BY-2 cells

Incubation experiments were conducted in a phosphate-deficient MS medium, herein referred as MS_{red} (phosphate concentration of 12.5 µM equals 1 % of original concentration), in order to reduce the precipitation of insoluble Eu(III)-phosphate. 1 mL of cell suspension that has been cultured for 96 h in standard nutrient medium was transferred into an 100 mL Erlenmeyer flask filled with 30 mL MS_{red} medium and the respective amount of Eu(III) stock solution ($EuCl_3 \cdot 6\ H_2O$ in MilliQ water). Cells were left for incubation under culture conditions and samples were taken after defined periods. Each sample was centrifuged at 3,000 *g* for 10 min at 4 °C in 1.5 mL-Eppendorf tubes. After separation from the cell pellet 1 mL of the supernatant was acidified with 10 µL of distilled HNO_3. Eu(III) content was assessed by ICP-MS with a NexION 350x spectrometer (Perkin Elmer, Rodgau, Germany)), indirectly providing information on the amount of bioassociated Eu(III) by recalculation. In total, five independent experiments were conducted.

To assess cell survival after Eu(III) contact, the Evans Blue viability assay[43] was conducted according to Rajabi *et al*.[34] Cells were separated from the respective medium by filtration into 12-well plates using a nylon membrane with 37 µm pore size fixed in CellCrown™ inserts (Sigma-Aldrich, Taufkirchen, Germany). Staining was carried out for 3 min with a 2.5% (w/v) aqueous solution of Evans Blue followed by washing the cells three times for 3 min with MS_{red} medium. Cells were observed in phase contrast imaging mode with an Olympus BX-61 microscope (Olympus, Hamburg, Germany) using a

Fuchs-Rosenthal (Brand GmbH & CO KG, Wertheim, Germany) counting chamber. Per sample, 300 cells were counted in three iterations. Incubation experiments with Gd(III) and Sm(III) were also carried out in phosphate-deficient MS medium (30 mL) with the respective amount of Gd(III) or Sm(III) stock solution, made from $GdCl_3 \cdot 6\ H_2O$ and $SmCl_3 \cdot 6\ H_2O$, respectively, dissolved in MilliQ water, to obtain a final concentration of 100 µM. The separation of cells from the supernatant was conducted as described above.

2.3. TRLFS approach

TRLFS was used to obtain information about the temporal change of Eu(III) speciation throughout the exposure of BY-2 cells. To consider only cell-associated Eu(III), cell pellets of each sample were washed twice with deionized water and analyzed in a 1.5 mL-Eppendorf tube. TRLFS spectra were acquired with a pulsed diode pumped Nd:YAG-OPO laser (EKSPLA NT230-50-SH/SF-SCU) and an excitation wavelength of 394 nm. After passing the spectrometer (Shamrock SR-303i-A, grating: 300 l/mm), the emitted luminescence light was detected by an ICCD camera (Andor iStar DH320T-18U-63) tempered to -35 °C. Spectra were recorded with an initial delay of 10 µs to the laser pulse in a spectral range of 500 to 780 nm with 200 accumulations per spectrum and time.
In order to extract distinct single Eu(III) species and their distributions along a parameter, TRLFS data were deconvoluted by the means of parallel factor analysis (PARAFAC) as described elsewhere.[44–46]

2.4. Chemical microscopy of Eu(III) in BY-2 cells

In order to preserve the cell structure and contents of Eu(III) exposed BY-2 cells for chemical microscopy, a fixation protocol with paraformaldehyde (PFA) was employed. Therefore, 1 mL of the incubated cell culture was transferred into a 1.5 mL-Eppendorf tube and gently centrifuged for 3 min at 1,000 *g*. Upon separation of the supernatant, the cell pellet was washed three times with an isotonic buffer solution containing 50 mM tris(hydroxymethyl)amino-methane and 0.25 M mannitol at pH 8 and subsequently fixed at 25 °C for at least 1 h with a 4% PFA solution in the aforementioned buffer. Before microscopy, the fixed cells were washed three times with the buffer solution to avoid handling with toxic PFA at the microscope.
The spatial distribution and speciation of Eu(III) in exposed BY-2 cells was subsequently probed with a Raman microscope (LabRAM system, Horiba Jobin Yvon, Lyon, France), equipped with external 532 nm Nd-YAG laser and 633 nm HeNe laser as light source. The laser beam was coupled into an Olympus BX-40 microscope and directed through an objective with 10-fold, 50-fold or 100-fold magnification. Eu(III) luminescence and Raman signals were gathered with the same objective and guided through a 200 µm pinhole to a spectrometer with 300 l/mm grating and 200 µm entrance slit width before eventually reaching a Peltier cooled (-70 °C) CCD detector. Data acquisition in the range of 560 to 725 nm and optional baseline correction was carried out with LabSpec 5 software (Horiba Jobin Yvon). The dataset derived from chemical microscopy was deconvoluted by the means of a non-negative iterative factor analysis (NIFA) as described elsewhere.[47]

2.5. Oxalate synthesis

Eu(III)-oxalate was prepared according to Alexander *et al.*[48]
For the synthesis of Ca(II)-oxalate crystals, the abovementioned procedure was adapted accordingly. 5 mL 0.15 M oxalic acid were added to 5 mL 0.5 M NaCl solution, stirred at 900 rpm and heated to 75 °C. Dropwise addition of 5 mL 0.1 M $CaCl_2$ to this solution yielded a white precipitate. After 10 min of stirring at 75°C, the precipitate was separated by centrifugation, washed twice with deionized water, once with acetone and subsequently dried at 75 °C.

3. Results and discussion

3.1. Eu(III) uptake and effect on cell viability

Time-dependent bioassociation experiments were performed to gain insights into the interaction of tobacco BY-2 cells with Eu(III). For this purpose, a concentration of 100 µM Eu(III) was applied in experimental series. In order to examine the effect of Eu(III) on cell viability, the Evans Blue dye test was performed on metal-incubated and control cells. The assay is based on the penetration of the dye through the cell membrane of BY-2 cells, which lost their membrane integrity and hence are considered non-viable anymore. Within the first five hours of incubation, the viabilities of metal-exposed and control cells are comparable (see **Fig. 1**). While the viability of the control cells stayed above 95% throughout the entire incubation time, the viability of Eu(III) exposed cells, decreases with exposure time to values of 89±2% after 24 h and 69±11% after 144 h.
In similar experiments with U(VI) and BY-2 cells conducted by Rajabi *et al.*,[34] a concentration of 50 µM U(VI) was already regarded as toxic and led to viabilities of ≈30% after 96 h. In contrast, BY-2 cells can cope with concentrations of 100 µM

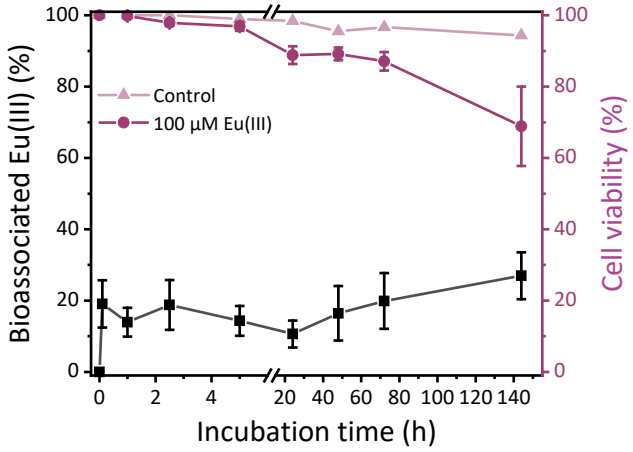

Fig. 1: Bioassociation of Eu(III) onto tobacco BY-2 cells and cell viability upon exposure to 100 µM Eu(III) compared to untreated cells (control) over a time period of 144 h. Data represent mean values and standard deviation (SD) from three independent experimental series.

Eu(III) without considerable loss of viability. This might be explained by the bioavailability of Eu(III) in the medium. In the beginning, the Eu(III)-aquo ion, the bioavailable form of Eu(III), is the dominating species in solution (see ESI, **Fig S 2**), whereas an increase of the share of a second liquid Eu(III) species, most probably the less bioavailable Eu(III)-EDTA, can be observed.

Analysis of Eu(III) concentration in the supernatant shows that bioassociation immediately starts upon exposing BY-2 cells to the Eu(III)-containing MS_{red} medium. This initial and rapid increase (see **Fig. 1**) can be attributed to the passive and thus instantaneous process of biosorption of the Eu(III)-aquo ion on the exterior of the cell walls, in which 19±7% of the metal is bioassociated. Due to attractive forces between the positively charged metal and negatively charged functional groups, *e.g.* carboxyl and phosphate groups, it is likely that Eu(III) is sorbed on the cell wall surface independent of the cell's metabolism. However between 24 h and 144 h incubation time, the amount of bioassociated Eu(III) is slowly increasing up to 27±7%.

It was further investigated whether Eu(III) speciation changes throughout the incubation time as well. Therefore, a time-resolved spectroscopic approach was applied.

3.2. Time-resolved speciation change in BY-2 cells

Subsequent to the quantitative description of Eu(III) bioassociation, a spectroscopic investigation on the chronological Eu(III) speciation alteration within the BY-2 cells was conducted. Therefore, washed cell pellets of BY-2 cells, incubated with 100 µM Eu(III) for variable periods, were analysed by TRLFS and data deconvoluted by the means of PARAFAC.

Within the examined incubation period, a substantial change of luminescence spectra was observed. Thorough separation of the sum spectra results in two clearly distinguishable luminescent single components. Component 1, coloured in orange in **Fig. 2,** is the dominating Eu(III) species within the first few hours of incubation and exhibits a luminescence lifetime of τ_1=190 µs. It can be detected directly after the first contact of Eu(III) and the BY-2 cells (corresponds to sample t=0). This result implies an instantaneous bioassociation event, which is in accordance with the results in section **3.1**. Therein, a passive and hence rapid sorption via surface complexation of the Eu(III)-aquo ion to functional groups (*e.g.* carboxylate groups) on the cell wall or outer layers was suspected which herewith was validated spectroscopically in terms of time.

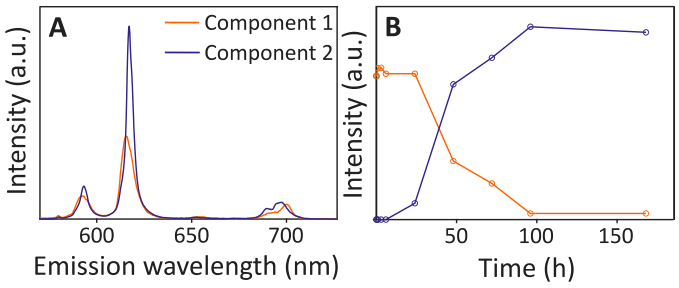

Fig. 2: Deconvolution results from TRLFS data of the time-dependent incubation of BY-2 cells with 100 µM Eu(III), derived from PARAFAC. **A** Normalized single component spectra of Eu(III) species present in BY-2 cells, **B** Species distribution in dependence on exposure time.

Between 24 and 48 h exposure time, a significant transition from one cell-associated component into another occurs, which is explicitly accompanied by a change of peak intensity ratios and peak shape. From 48 h onwards, component 2 (depicted in blue in **Fig. 2**) is dominating the luminescence spectra while the share of component 1 is simultaneously decreasing. Fitting the luminescence decay results in a lifetime of τ_2=219 µs. The respective decay curves can be found in the ESI, **Fig. S 3**.

Although no qualitative assignment of Eu(III) species can be made in here, it provides an evidence for a time-dependent emergence of a second cell-associated component, which is directly associated with the transition from the initial dominant luminescence one.

This macroscopic insight lead us to conclude that the Eu(III)–BY-2 system is subject to several underlying metal bioassociation processes. Therefore, an examination on the microscopic level is indispensable.

3.3. Spatial distribution of Eu(III) in BY-2 cells

In order to resolve the location and distribution of the previously described Eu(III) components, chemical microscopy has been applied for cells incubated with 100 µM Eu(III) for different time intervals. Therefore, physiologically intact cells were chosen and point measurements were conducted at different intracellular compartments, *e.g.* cell wall, nucleus, endoplasmatic reticulum and vesicles. The data reveal characteristic and distinguishable Eu(III) luminescence signals at some of these compartments already after 24 h exposure time (see ESI, **Fig. S 4**). This indicates that, beside a suspected extracellular biosorption, metal uptake processes into the cells are also occurring within the first 24 h, whereas prolonged incubation times usually led to an increase of Eu(III) luminescence intensities.

Building on these investigations, microspectroscopic mapping was performed to obtain comprehensive luminescence information not solely from single compartments but entire cells. Therefore, BY-2 cells incubated for 48 h with 100 µM Eu(III) were chosen and fixed as described in section **2.4**. Spectral data show strong Eu(III) luminescence intensities in several hotspot regions. Data deconvolution on the basis of spectral features was performed with NIFA and revealed the presence of four distinct Eu(III) species – two species more than we found in the TRLFS data of cell pellets – of which one strongly resembles the emerging blue component from bulk TRLFS measurements (see **Fig. 3**). This highlights the strength of the applied procedure, since strong local differences in the occurrence of certain components throughout the cell enable an enhanced separation of diverse Eu(III) coordination environments.

3.3.1. Species 1

Species 1, shown in **Fig. 3** in yellow, stands out with peculiar occurrence at the cell's nucleus, a cellular compartment that is easily identifiable due to its spherical shape, and nucleolus (see species distribution maps in ESI, **Fig. S 5**). The nucleus directs cellular activities, *e.g.* cell growth and differentiation, and holds

the genetic material in a condensed form called chromatin, which consists of deoxyribonucleic acid (DNA) and special proteins. The affinity of Eu(III) to nucleic acids is well known.[49] In combination with its excellent luminescence properties, it gives rise to applications such as fluorescent DNA labelling.[50] It has also been shown by TRLFS studies that Eu(III) is able to coordinate the phosphatic oxygens of the DNA backbone.[51] Comparison of the spectrum of species 1 with various literature data for Eu(III) spectra in the presence of nucleic acids, with extracellular DNA of a microorganism[47] and DNA origami nanostructures[52] reveals concise similarities in the spectral characteristics, which are a pronounced shoulder in the $^5D_0 \rightarrow {}^7F_2$ signal (see ESI, **Fig. S 1**), the shape of $^5D_0 \rightarrow {}^7F_4$ band and F_2/F_1 ratio. Hence, species 1 likely represents a Eu(III) coordination with organic phosphate groups of DNA or ribonucleic acids (RNA).

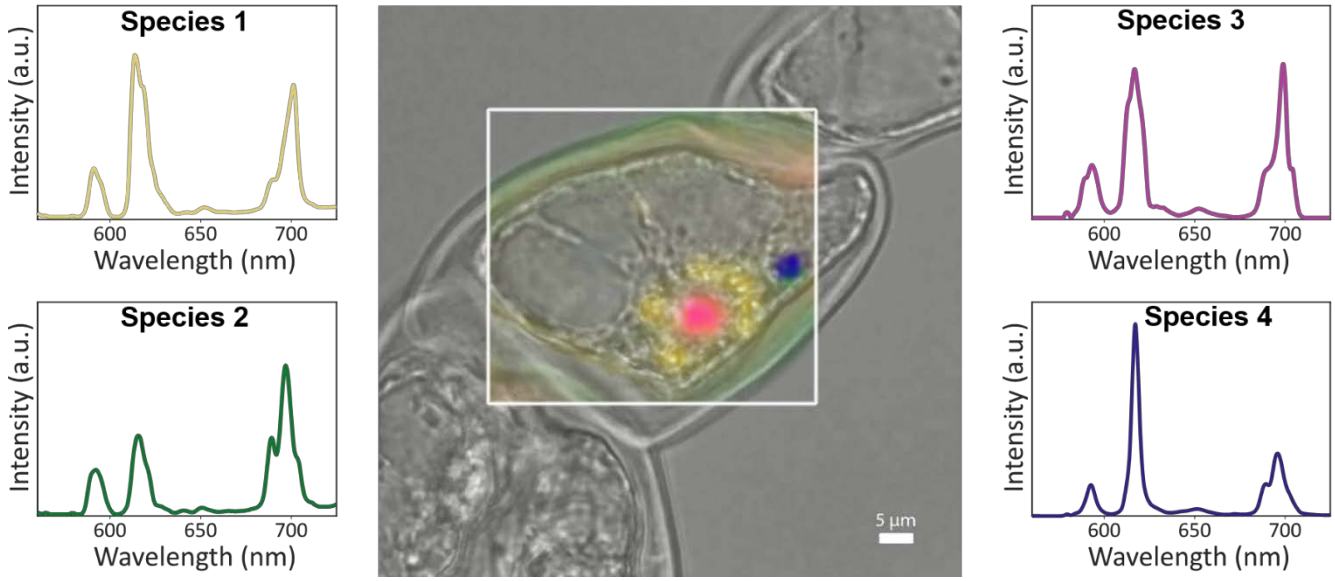

Fig. 3: Single component luminescence spectra and microscopic image with local distribution of respective Eu(III) species, derived from NIFA. Cells were incubated for 48 h with 100 µM Eu(III) and fixed with PFA for chemical microscopy.

3.3.2. Species 2

Another cell compartment for Eu(III) accumulation, where the species 2 shown in green in **Fig. 3** was detected, is the cell wall separating the intracellular area from the surrounding medium. Plant cell walls are composed of polysaccharide polymers, namely cellulose, hemicellulose and pectin as well as smaller portions of glycoproteins. The affinity of carbohydrates for Ln has been reported in the literature and is based on the presence of carboxylate groups, being hard bases, which willingly complexate Ln cations, which are usually hard acids.[53] Beside carboxylates, also hydroxyl groups, *e.g.* in galacturonic acids, form stable complexes with Eu(III).[54] Especially pectin – an acidic heteropolysaccharide – contains many galacturonic acid units with negative charge that are compensated by a hydration sphere and cations like Ca(II).[55]

The spectrum of this species cannot be clearly assigned to one single spectroscopic reference. However, because of the cumulative occurrence of species 2 at the BY-2's cell walls and the capability of the higher charged Eu(III) to displace Ca(II) from certain binding centers,[15] a potential coordination of the Ln to negatively charged carboxylate and hydroxyl groups of, for instance, polysaccharides can be suspected herein.

3.3.3. Species 3

A third Eu(III) species (see magenta species in **Fig. 3**) differs spectroscopically from the other species in terms of F_2/F_1 ratio and $^5D_0 \rightarrow {}^7F_4$ band shape. Beside its slight occurrence at the cell membrane (see ESI, **Fig. S 5**), this Eu(III) species is particularly dominant in the nucleolus of the cell. Besides its primary role as the site of ribosome biogenesis, the nucleolus is involved in the regulation of mitosis and cellular stress responses.[56] It has been shown that metal ion stress (*e.g.* by Cd, Pb, Cu, Hg, Al) can affect the nucleolar structure and its function, leading to irregularly shaped nucleoli and extrusion of its interior into the cytoplasm.[57,58] No such morphological alteration of the nucleolus was observed in the cell under examination, though a leakage cannot be excluded with the applied techniques. However, the nucleolus offers several binding environments like phosphorylates proteins and RNA. Coordination of Eu(III) to proteinaceous structures involve either replacement of Ca(II) at its binding site or a binding to carboxylate residues.[15] Though a precise specification of the coordinating ligand is not straightforward, Eu(III) species 3 can be denoted to a protein-bound binding motif.

3.3.4. Species 4

Species 4, shown in blue in **Fig. 3**, stands out by a noticeably narrow spectral bandwidth with a pronounced $^5D_0 \rightarrow {}^7F_2$ signal. In fact, the luminescence intensity of this transition is five times higher than in any other spectrum acquired in this microspectroscopic mapping. Additionally, the spectrum of this species matches perfectly with the one deconvoluted from TRLFS data in the previous section, therein referred to as 'second cell-associated species'. According to the distribution map, this prominent Eu(III) species occurs exclusively at one

particular site in the cell. A detailed consideration of the microscopic image at the respective site of occurrence reveals a clearly distinguishable crystal-like structure with a size of 4 µm. Single point measurements confirmed that this particular compartment gives rise to such strong luminescence signals. Subsequent differential interference contrast microscopy revealed the occurrence of such structures in almost every cell (see ESI, **Fig. S 5**).

Since an unambiguous identification of the Eu(III)-coordinating ligand on the basis of the luminescence spectrum is rather complicated, species 4 was examined more in detail in successive investigations.

Remarkably, chemical microscopy allowed herein the retrieval of the sharp signal spectrum (species 4) that has already been observed in TRLFS measurements (component 2) and enabled the spatial resolution of single species that could not be unravelled by TRLFS of bulk cells.

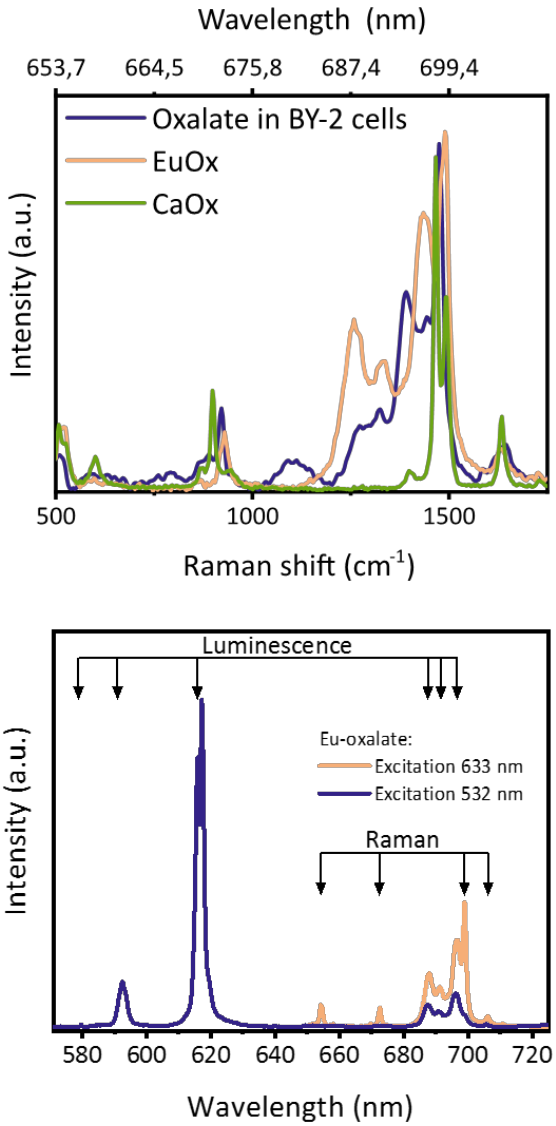

Fig. 4: Raman and luminescence spectra of oxalates. **Top:** Raman spectra of Eu(III)-containing crystal-like structure in BY-2 cells and two synthesised reference compounds (EuOx and CaOx), obtained upon excitation with 633 nm. **Bottom:** Assignment of Raman and luminescence bands of synthesised EuOx upon excitation with different wavelengths.

3.4. Species characterization by Raman microspectroscopy

In order to obtain more chemical information about the crystal-like compartment found in the BY-2 cell and to mitigate Eu(III) photoluminescence, excitation wavelength was changed to 633 nm and spectra were recorded at the luminescence hotspot of species 4 with particular focus on the Raman fingerprint region. Database search of the resulting Raman spectrum shows hints for the oxalate minerals weddellite and whewellite, which is hydrated Ca(II)-oxalate ($Ca(C_2O_4)\cdot(2.5\text{-}x)H_2O$ with $0 \le x \le 0.25$ and $Ca(C_2O_4)\cdot H_2O$, respectively.[59,60] Calcium oxalates (CaOx) are among the most abundant biominerals in nature and serve as storage of excess intracellular Ca in order to maintain a low free Ca concentration in the cytoplasm. Beside this, they might play a role in herbivory defense and mechanical support. The process of oxalate biomineralization, however, is related to heavy metal tolerance, as reported in a variety of studies with different plant species.[61–66]

On the basis of similar ionic radii of Ca(II) and Eu(III) and because of the good accordance of the Raman spectrum from a readily prepared CaOx (see **2.5**) with the one of the Eu(III)-containing crystal-like structure in BY-2 cells, shown in **Fig. 4**, one can assume that the latter consist, at least partially, of Eu(III)-oxalate. In order to further support this hypothesis, powderous Eu(III)-oxalate decahydrate (EuOx)[47] was probed by chemical microscopy. Both, the synthesised oxalates CaOx and EuOx, as well as the crystallites in BY-2 cells are characterised by distinctive Raman spectral features: A very intense band at ~1480 cm^{-1}, corresponding to C=O stretching mode, and moderate bands at ~1640 cm^{-1}, ~920 cm^{-1} (C–C stretching mode) and ~512 cm^{-1} (M–O stretching mode) are in good agreement with Morris *et al.*, who scrutinized Raman spectra of Ln oxalates.[67] Slight shifts in vibrational frequencies between the reference from the literature, the synthesised oxalates and the Eu(III) containing crystallites in BY-2 cells can be attributed to a variation in the degree of covalency of the metal-oxygen bonding as well as the nature and charge of the coordinated metal ion.

Beside the already interpreted Raman signals in **Fig. 4**, several unclassified peaks at ~1439 cm^{-1}, ~1366 cm^{-1} and ~1268 cm^{-1} occur in the spectra of EuOx and the oxalates in BY-2 cells which can be traced back to the luminescence of the $^5D_0 \rightarrow {}^7F_4$ transition of Eu(III).

While the synthesised oxalates solely comprise of either Eu(III) or Ca(II) as cation, the oxalate in BY-2 cells was precipitated from the cytoplasm or cell sap which additionally contains a variety of different cations, *e.g.* Mg and K, enzymes, inorganic and organic molecules. A mix of oxalates with different cations beside Eu(III), different waters of crystallisation or even a ternary system cannot be excluded herein.

Remarkably, light microscopic and spectroscopic analysis of multiple Eu(III)-incubated BY-2 cells reveal the presence of one Eu(III) oxalate biomineral per cell in almost every cell under observation (see ESI, **Fig. S 6**). They appear in various morphologies, *e.g.* as rods, hexagonal plates, rhombohedrons or pyramids. These consistent results suggest that the

formation of oxalates in which the non-essential Eu(III) is embedded is a sequestration pathway for potentially toxic metals, since a deposition in biominerals makes them physiologically harmless for BY-2 cells. It is commonly known that Pb,[63,66] Sr,[61,63,64] Cd,[63,68] Cu,[62] and Al[62,69] are incorporated into oxalate crystals as internal detoxification mechanism. To the best of our knowledge, no such coping mechanism has been reported for Ln in plants or plant cells so far. Further experiments with other Ln than Eu(III), namely Gd(III) and Sm(III), show exactly the same results (see ESI, **Fig. S 7**), indicating the existence of this particular metal detoxification pathway by biomineralization of oxalates.

Conclusions

In this study, the uptake and spatial distribution of Eu(III) in a suspension cell culture of tobacco BY-2 was examined. The results indicate a phased but not quantitative bioassociation of up to 27±7% of 100 µM Eu(III) without a considerable loss of cell viability. Time-dependent spectroscopic measurements of Eu(III) afflicted BY-2 cell pellets revealed a staggered occurrence of two distinct cell-associated Eu(III) components. The first of which appears directly after metal–cell contact and converts into the second component with characteristically narrow Eu(III) emission bands in subsequent days. Thorough microscopic examination of Eu(III) exposed cells by chemical microscopy in combination with NIFA allowed for the resolution of four distinct Eu(III) single component spectra, *i.e.* varying intracellular Eu(III) binding environments. Cellular binding sites within the cell's nucleus and cell membranes are phosphate groups which coordinate Eu(III). Another species which is primarily located at the cell wall is highly likely corresponding to carboxylate and/or hydroxide coordinated Eu(III). Furthermore, the nucleolus was identified as an prominent site of Eu(III) bioaccumulation and suggests a protein-bound metal species. A fourth spectral species, occurring solely at one particular site within the cell, matches perfectly with the gradually emerging component found by TRLFS measurements. Thorough analysis of the compartment of interest by Raman microscopy indicated an oxalate-containing biomineral. Further bioassociation experiments with Gd(III) and Sm(III) prove the formation of oxalate crystals within the BY-2 cells.

Herein, we hypothesize a biomineralization of Ln(III)-containing oxalates as a way for tobacco BY-2 cells to successfully cope with an excess of free metal ions. Our results clearly show that, despite existing and partly effective detoxification mechanisms, Ln are simultaneously traceable in other binding forms in different parts of the cell due to their similarity to Ca(II). Therefore, it must be assumed that the toxic effect of Ln is possibly very complex.

This work has, for the first time, revealed biomineralization as basic detoxification process for Ln ions in tobacco BY-2 cells. The results not only enhance our understanding of the underlying molecular processes, but contribute to an extensive knowledge of biogeochemical cycles of Ln as well. Following this, future research should employ the use of entire plants in order to elucidate similar mechanisms in more sophisticated organisms. Additionally, the applied workflow of chemical microscopy and data deconvolution has proven its strength herein and should also be applied to other Ln-plant-systems in the future.

Author Contributions

Max Klotzsche: conceptualization, investigation, data curation, validation, visualization writing – original draft. Manja Vogel: conceptualization, supervision, validation, visualization, writing – review & editing. Susanne Sachs: resources, writing – review & editing. Johannes Raff: funding acquisition, writing – review & editing. Thorsten Stumpf: resources, supervision. Björn Drobot: conceptualization, formal analysis, methodology, software, supervision, visualization, writing – review & editing. Robin Steudtner: conceptualization, project administration, supervision, writing – review & editing.

Conflicts of interest

There are no conflicts to declare.

Acknowledgements

The first batch of BY-2 cells was kindly provided by Prof. P. Nick from the Botanical Institute, Karlsruhe Institute of Technology. The research was funded by the Federal Ministry of Education and Research as part of the joint project "RENA" (Biological remediation by natural association processes) under contract number 02NUK066A and 02NUK066D. The authors thank S. Beutner for multiple ICP-MS measurements, J. Seibt for cultivation support and H. Moll for fruitful discussions.

References

1 V. Balaram, *Geoscience Frontiers*, 2019, **10**, 1285–1303.

2 D. H. Dang, K. A. Thompson, L. Ma, H. Q. Nguyen, S. T. Luu, M. T. N. Duong and A. Kernaghan, *Arch Environ Contam Toxicol*, 2021, **81**, 521–530.

3 S. Kulaksiz and M. Bau, *Earth Planet Sci Lett*, 2013, **362**, 43–50.

4 V. González, D. A. L. Vignati, M. N. Pons, E. Montarges-Pelletier, C. Bojic and L. Giamberini, *Environmental Pollution*, 2015, **199**, 139–147.

5 A. D. Kotelnikova, O. B. Rogova and V. V. Stolbova, *Eurasian Soil Science 2021 54:1*, 2021, **54**, 117–134.

6 J. Zhang, Z. Wang, Q. Wu, Y. An, H. Jia and Y. Shen, *International Journal of Environmental Research and Public Health 2019, Vol. 16, Page 4052*, 2019, **16**, 4052.

7 I. Kim, Kim and I., *AGUFM*, 2019, **2019**, H41J-1842.

8 P. Louis, A. Messaoudene, H. Jrad, B. A. Abdoul-Hamid, D. A. L. Vignati and M. N. Pons, *Science of The Total Environment*, 2020, **742**, 140619.

9 B. Wei, Y. Li, H. Li, J. Yu, B. Ye and T. Liang, *Ecotoxicol Environ Saf*, 2013, **96**, 118–123.

10 X. Li, Z. Chen, Z. Chen and Y. Zhang, *Chemosphere*, 2013, **93**, 1240–1246.

11 A. M. Khan, N. Kartini, A. Bakar, A. Farid and M. A. Ashraf, *RECENT ADVANCES IN ASSESSMENT ON CLEAR WATER, SOIL AND AIR*, , DOI:10.1007/s11356-016-7427-1.

12 R. Singh, N. Gautam, A. Mishra and R. Gupta, *Indian J Pharmacol*, 2011, **43**, 246.

13 E. J. Martinez-Finley, S. Chakraborty, S. J. B. Fretham and M. Aschner, *Metallomics*, 2012, **4**, 593–605.

14 T. Dudev and C. Lim, *Chem Rev*, 2014, **114**, 538–556.

15 B. Drobot, M. Schmidt, Y. Mochizuki, T. Abe, K. Okuwaki, F. Brulfert, S. Falke, S. A. Samsonov, Y. Komeiji, C. Betzel, T. Stumpf, J. Raff and S. Tsushima, *Physical Chemistry Chemical Physics*, 2019, **21**, 21213–21222.

16 F. Tommasi, P. J. Thomas, G. Pagano, G. A. Perono, R. Oral, D. M. Lyons, M. Toscanesi and M. Trifuoggi, *Arch Environ Contam Toxicol*, 2021, **81**, 531–540.

17 C. de Oliveira, S. J. Ramos, J. O. Siqueira, V. Faquin, E. M. de Castro, D. C. Amaral, V. H. Techio, L. C. Coelho, P. H. P. e Silva, E. Schnug and L. R. G. Guilherme, *Ecotoxicol Environ Saf*, 2015, **122**, 136–144.

18 S. M. Ramírez-Olvera, L. I. Trejo-Téllez, S. García-Morales, J. A. Pérez-Sato and F. C. Gómez-Merino, *PLoS One*, 2018, **13**, e0194691.

19 S. Clemens, *Planta*, 2001, **212**, 475–486.

20 J. L. Hall, *J Exp Bot*, 2002, **53**, 1–11.

21 N. Bazihizina, C. Taiti, L. Marti, A. Rodrigo-Moreno, F. Spinelli, C. Giordano, S. Caparrotta, M. Gori, E. Azzarello and S. Mancuso, *J Exp Bot*, 2014, **65**, 4931–4942.

22 À. Carrió-Seguí, P. Romero, C. Curie, S. Mari and L. Peñarrubia, *Scientific Reports 2019 9:1*, 2019, **9**, 1–14.

23 A. Jogawat, B. Yadav, Chhaya and O. P. Narayan, *Physiol Plant*, 2021, **173**, 259–275.

24 G. Nagahashi, W. W. Thomson and R. T. Leonard, *Science (1979)*, 1974, **183**, 670–671.

25 H. Quiquampoix, R. G. Ratcliffe, S. Ratković, S. Ratković and Ž. Vučinić, *J Inorg Biochem*, 1990, **38**, 265–275.

26 F. Han, X.-Q. Shan, J. Zhang, Y.-N. Xie, Z.-G. Pei, S.-Z. Zhang, Y.-G. Zhu and B. Wen, *New Phytol*, 2005, **165**, 481–492.

27 Z. Wei, F. Hong, M. Yin, H. Li, F. Hu, G. Zhao and J. W. Wong, *Biol Trace Elem Res*, 2005, **106**, 279–297.

28 S. Zheng, C. Zhang, K. Shi, J. Wang, G. Sun, Q. Hu, F. Zhao and X. Wang, *Journal of Rare Earths*, 2018, **36**, 331–336.

29 J. Jessat, H. Moll, W. A. John, M. L. Bilke, R. Hübner, J. Kretzschmar, R. Steudtner, B. Drobot,

T. Stumpf and S. Sachs, *J Hazard Mater*, 2022, **439**, 129520.

30 J. Jessat, W. A. John, H. Moll, M. Vogel, R. Steudtner, B. Drobot, R. Hübner, T. Stumpf and S. Sachs, *Ecotoxicol Environ Saf*, 2023, **254**, 114741.

31 S. Sachs, G. Geipel, F. Bok, J. Oertel and K. Fahmy, *Environ Sci Technol*, 2017, **51**, 10843–10849.

32 H. Moll, M. Schmidt and S. Sachs, *J Hazard Mater*, 2021, **412**, 125251.

33 W. A. John, B. Lückel, N. Matschiavelli, R. Hübner, S. Matschi, W. Hoehenwarter and S. Sachs, *Science of The Total Environment*, 2022, **823**, 153700.

34 F. Rajabi, J. Jessat, J. N. Garimella, F. Bok, R. Steudtner, T. Stumpf and S. Sachs, *Ecotoxicol Environ Saf*, 2021, **211**, 111883.

35 J. Jessat, S. Sachs, H. Moll, W. John, R. Steudtner, R. Hübner, F. Bok and T. Stumpf, *Environ Sci Technol*, 2021, **55**, 6718–6728.

36 T. Nagata, Y. Nemoto and S. Hasezawa, *Int Rev Cytol*, 1992, **132**, 1–30.

37 T. Raeymaekers, G. Potters, H. Asard, Y. Guisez and N. Horemans, *Protoplasma*, 2003, **221**, 93–100.

38 P. L. Gratão, G. B. Pompeu, F. R. Capaldi, V. A. Vitorello, P. J. Lea and R. A. Azevedo, *Plant Cell Tissue Organ Cult*, 2008, **94**, 73–83.

39 Z. Poborilova, R. Opatrilova and P. Babula, *Environ Exp Bot*, 2013, **91**, 1–11.

40 O. Krystofova, J. Sochor, O. Zitka, P. Babula, V. Kudrle, V. Adam and R. Kizek, *International Journal of Environmental Research and Public Health 2013, Vol. 10, Pages 47-71*, 2012, **10**, 47–71.

41 L. Svobodníková, M. Kummerová, Š. Zezulka and P. Babula, *Ecotoxicol Environ Saf*, 2019, **182**, 109369.

42 Y. Dai, J. Zhao, X. Liu, X. Yu, Z. Jiang, Y. Bu, Z. Xu, Z. Wang, X. Zhu and B. Xing, *Environ Sci Nano*, 2019, **6**, 2724–2735.

43 D. F. Gaff and O. Okong'o-ogola, *J Exp Bot*, 1971, **22**, 756–758.

44 C. A. Andersson and R. Bro, *Chemometrics and Intelligent Laboratory Systems*, 2000, **52**, 1–4.

45 B. Drobot, R. Steudtner, J. Raff, G. Geipel, V. Brendler and S. Tsushima, *Chem Sci*, 2015, **6**, 964–972.

46 B. Drobot, A. Bauer, R. Steudtner, S. Tsushima, F. Bok, M. Patzschke, J. Raff and V. Brendler, *Anal Chem*, 2016, **88**, 3548–3555.

47 M. Vogel, R. Steudtner, T. Fankhänel, J. Raff and B. Drobot, *Analyst*, 2021, **146**, 6741–6745.

48 D. Alexander, K. Thomas, M. Joy, P. R. Biju, N. V. Unnikrishnan and C. Joseph, *Acta Crystallogr C Struct Chem*, 2019, **75**, 589–597.

49 C. H. Evans, *Biochemistry of the Lanthanides*, 1990, 85–172.

50 N. Sabbatini, M. Guardigli and I. Manet, *Handbook on the Physics and Chemistry of Rare Earths*, 1996, **23**, 69–119.

51 S. L. Klakamp and W. D. Horrocks, *Biopolymers*, 1990, **30**, 33–43.

52 L. Opherden, J. Oertel, A. Barkleit, K. Fahmy and A. Keller, *Langmuir*, 2014, **30**, 8152–8159.

53 B. Gyurcsik and L. Nagy, *Coord Chem Rev*, 2000, **203**, 81–149.

54 H. Grasdalen and T. Anthonsen, , DOI:10.3891/acta.chem.scand.40b-0735.

55 B. Alberts, A. Johnson, J. Lewis, M. Raff, K. Roberts and P. Walter, in *Molecular Biology of the Cell*, Garland Science, New York, 4th edition., 2002.

56 F. M. Boisvert, S. Van Koningsbruggen, J. Navascués and A. I. Lamond, *Nature Reviews Molecular Cell Biology 2007 8:7*, 2007, **8**, 574–585.

57 L. Zhaib, W. Jiang and W. Wang, *Isr J Plant Sci*, 1995, **43**, 125–133.

58 M. G. F. Lima, L. C. Rocha, G. L. Silveira, I. F. S. Alvarenga and L. F. Andrade-Vieria, *Ecotoxicol Environ Saf*, 2019, **174**, 630–636.

59 C. Sterling, *Acta Cryst.*, 1965, **18**, 917–921.

60 H. J. Arnott, F. G. E. Pautard and H. Steinfink, *Nature 1965 208:5016*, 1965, **208**, 1197–1198.

61 V. R. Franceschi and A. M. Schueren, *Protoplasma*, 1986, **130**, 199–205.

62 A. M. A. Mazen, *Russian Journal of Plant Physiology*, 2004, **51**, 281–285.

63 A. M. A. Mazen and O. M. O. El Maghraby, *Biol Plant*, 1997, **40**, 411–417.

64 E. Zindler-Frank, *Botanica Acta*, 1991, **104**, 229–232.

65 Y. E. Choi, E. Harada, M. Wada, H. Tsuboi, Y. Morita, T. Kusano and H. Sano, *Planta*, 2001, **213**, 45–50.

66 Y. Y. Yang, J. Y. Jung, W. Y. Song, H. S. Suh and Y. Lee, *Plant Physiol*, 2000, **124**, 1019–1026.

67 D. E. Morris and D. E. Hobart, *Journal of Raman Spectroscopy*, 1988, **19**, 231–237.

68 Y. E. Choi and E. Harada, *Journal of Plant Biology*, 2005, **48**, 113–119.

69 Jian Feng Ma, Shao Jian Zheng, H. Matsumoto and S. Hiradate, *Nature 1997 390:6660*, 1997, **390**, 569–570.